Problem Set 4: Analysis of the 2004 Sumatra-Andaman earthquake
Part 1: Instrument response and spectral analysis

GEOS 626: Applied Seismology, Carl Tape

Assigned: February 13, 2014 — Due: February 20, 2014

Last compiled: October 16, 2017

SOLUTIONS

Problem 1. Complex numbers and functions

1. Using $z = re^{i\theta}$ and $z^* = re^{-i\theta}$:

(a)

$$\begin{aligned} z &= z_1 z_2 = r_1 e^{i\theta_1}\ r_2 e^{i\theta_2} = r_1 r_2 e^{i\theta_1}\ e^{i\theta_2} = r_1 r_2 e^{i(\theta_1+\theta_2)} = re^{i\theta} \\ r &= r_1 r_2 \\ \theta &= \theta_1 + \theta_2 \end{aligned}$$

(b)

$$\begin{aligned} z &= z_1/z_2 = r_1 e^{i\theta_1}/(r_2 e^{i\theta_2}) = r_1 e^{i\theta_1} r_2^{-1} e^{-i\theta_2} = (r_1/r_2) e^{i(\theta_1-\theta_2)} = re^{i\theta} \\ r &= r_1/r_2 \\ \theta &= \theta_1 - \theta_2 \end{aligned}$$

(c)

$$\begin{aligned} (z_1 z_2)^* &= (r_1 e^{i\theta_1}\ r_2 e^{i\theta_2})^* \\ &= (r_1 r_2 e^{i(\theta_1+\theta_2)})^* \\ &= r_1 r_2 e^{-i(\theta_1+\theta_2)} \\ &= r_1 r_2 e^{-i\theta_1} e^{-i\theta_2} \\ &= r_1 e^{-i\theta_1} r_2 e^{-i\theta_2} \\ &= z_1^* z_2^* \end{aligned}$$

(d) We know that $|z| = r$.

$$\begin{aligned} z^* z &= re^{i\theta} re^{-i\theta} = r^2 e^{i(\theta-\theta)} = r^2 \\ z^* z &= |z|^2 \\ \sqrt{z^* z} &= |z| \end{aligned}$$

Using $z = a + bi$ and $z^* = a - bi$:

(a)

$$\begin{aligned}
z &= z_1 z_2 \\
&= (a_1 + b_1 i)(a_2 + b_2 i) \\
&= a_1 a_2 + a_1 b_2 i + a_2 b_1 i + (b_1 i)(b_2 i) \\
&= a_1 a_2 + a_1 b_2 i + a_2 b_1 i - b_1 b_2 \\
&= (a_1 a_2 - b_1 b_2) + i(a_2 b_1 + a_1 b_2) \\
&= a + bi \\
a &= a_1 a_2 - b_1 b_2 \\
b &= a_2 b_1 + a_1 b_2
\end{aligned}$$

(b)

$$\begin{aligned}
z &= z_1 / z_2 \\
&= \frac{a_1 + b_1 i}{a_2 + b_2 i} \\
&= \frac{a_1 + b_1 i}{a_2 + b_2 i} \left(\frac{a_2 - b_2 i}{a_2 - b_2 i} \right) \\
&= \frac{a_1 a_2 - a_1 b_2 i + a_2 b_1 i - b_1 b_2 i^2}{a_2^2 + b_2^2} \\
&= \frac{a_1 a_2 + b_1 b_2 + i(a_2 b_1 - a_1 b_2)}{a_2^2 + b_2^2} \\
&= a + bi \\
a &= \frac{a_1 a_2 + b_1 b_2}{a_2^2 + b_2^2} \\
b &= \frac{a_2 b_1 - a_1 b_2}{a_2^2 + b_2^2}
\end{aligned}$$

(c)

$$\begin{aligned}
(z_1 z_2)^* &= [(a_1 + b_1 i)(a_2 + b_2 i)]^* \\
&= [(a_1 a_2 - b_1 b_2) + i(a_2 b_1 + a_1 b_2)] \\
&= [(a_1 a_2 - b_1 b_2) - i(a_2 b_1 + a_1 b_2)] \\
&= (a_1 a_2 - b_1 b_2) - i(a_2 b_1 + a_1 b_2) \\
&= a_1 a_2 - a_1 b_2 i - a_2 b_1 i + b_1 b_2 i^2 \\
&= (a_1 - b_1 i)(a_2 - b_2 i) \\
&= z_1^* z_2^*
\end{aligned}$$

(d) We know that $|z| = \sqrt{a^2 + b^2}$.

$$\begin{aligned} z^* z &= (a + bi)(a - bi) = a^2 - abi + abi - b^2 i^2 = a^2 + b^2 \\ z^* z &= |z|^2 \\ \sqrt{z^* z} &= |z| \end{aligned}$$

2. (a) The forward and inverse Fourier transforms are defined as[1]

$$\mathcal{F}[h(t)] = H(\omega) = \int_{-\infty}^{\infty} h(t)\, e^{-i\omega t}\, \mathrm{d}t \tag{S1}$$

$$\mathcal{F}^{-1}[H(\omega)] = h(t) = \frac{1}{2\pi} \int_{-\infty}^{\infty} H(\omega)\, e^{i\omega t}\, \mathrm{d}\omega\ . \tag{S2}$$

The Fourier transform of $\dot{h}(t)$ can be determined using integration by parts,

$$\int u\, dv = [u\, v] - \int v\, du,$$

with

$$\begin{aligned} dv &= \dot{h}(t)\, dt \\ u &= e^{-i\omega t} \\ v &= h(t) \\ du &= -i\omega\, e^{-i\omega t} dt \end{aligned}$$

Thus, we can write

$$\begin{aligned} \mathcal{F}\left[\dot{h}(t)\right] &= \int_{-\infty}^{\infty} \dot{h}(t)\, e^{-i\omega t}\, \mathrm{d}t \\ &= \left[h(t)\, e^{-i\omega t}\right]_{-\infty}^{\infty} - \int_{-\infty}^{\infty} h(t)\, (-i\omega)\, e^{-i\omega t}\, \mathrm{d}t \\ &= i\omega \int_{-\infty}^{\infty} h(t)\, e^{-i\omega t}\, \mathrm{d}t \\ &= i\omega\, \mathcal{F}[h(t)] \qquad \text{(S3)} \\ H_1(\omega) &= i\omega H(\omega)\ . \qquad \text{(S4)} \end{aligned}$$

The key step is to recognize that $h(t)$ evaluated at $\pm\infty$ is zero. Why? Well, Mathworld states that this occurs "if the function is bounded so that $\lim_{x\to\pm\infty} h(t) = 0$ (as any physically significant signal must be)..."

This process can be iterated for the nth derivative to yield

$$\begin{aligned} \mathcal{F}\left[h^{(n)}(t)\right] &= (i\omega)^n\, \mathcal{F}[h(t)] \qquad \text{(S5)} \\ H_n(\omega) &= (i\omega)^n H(\omega)\ . \qquad \text{(S6)} \end{aligned}$$

Note that (S3)–(S6) will depend on the Fourier convention.

(b) The units of $H(\omega)$ are the units of $h(t)$, multiplied by seconds ([h] s).

[1] These are the conventions used in *Dahlen and Tromp* (1998, p. 109) and *Stein and Wysession* (2003, Section 6.4.2).

The units of $H_n(\omega)$ are the units of $h^{(n)}(t)$, multiplied by seconds ($[h^{(n)}]$ s). So if $h(t)$ is displacement, then $n = 2$ will give accelleration as $h''(t)$, which has units of m s^{-2}. The units of $H_n(\omega)$ are then m s^{-1}.

3. The amplitude spectrum of $H_n(\omega)$ is

$$\begin{aligned}
|H_n(\omega)|^2 &= |(i\omega)^n H(\omega)|^2 \\
&= [(i\omega)^n H(\omega)]^*[(i\omega)^n H(\omega)] \\
&= [(i\omega)^n]^* H^*(\omega)(i\omega)^n H(\omega) \\
&= [(i\omega)^*]^n H^*(\omega)(i\omega)^n H(\omega) \\
&= (-i\omega)^n (i\omega)^n H^*(\omega) H(\omega) \\
&= (-i\omega i\omega)^n H^*(\omega) H(\omega) \\
&= (\omega)^{2n} A^2(\omega) \\
|H_n(\omega)| &= \omega^n A(\omega) \\
A_n(\omega) &= \omega^n A(\omega)
\end{aligned}$$

4. From the question, we have

$$\begin{aligned}
u &= \ln \omega && \text{(S7)} \\
g_n(u) &= \ln[e^{nu} A(e^u)] && \text{(S8)} \\
&= \ln(e^{nu}) + \ln(A(e^u)) && \text{(S9)} \\
&= nu + g_0(u) && \text{(S10)} \\
g_n'(u) &= n + g_0'(u) && \text{(S11)}
\end{aligned}$$

where the prime ($'$) represents differentiation with respect to u.

(a) Equation (S11) shows that the slope of the amplitude spectrum is increased by n, where n is the order of differentiation on $h(t)$. For example, let's say we have some $h(t)$ with corresponding $A(\omega)$. The slope of the amplitude spectrum will be $g_0'(u)$. We can then differentiate $h(t)$ n times, and the slope of the corresponding amplitude spectrum will be $n + g_0'(u)$. So for each $u = \ln \omega$, the slope will be steepened by n. It is a very elegant result and easy to remember!

Note that things get messier if you want the expressions in terms of ω. Note [2]

$$\begin{aligned} g_0'(u) &= \frac{d}{du}\left[\ln[e^{0u}A(e^u)]\right] \\ &= \frac{d}{du}\left[\ln[A(e^u)]\right] \\ &= \frac{1}{A(e^u)}\frac{d}{du}\left[A(e^u)\right] \\ &= \frac{1}{A(e^u)}A'(e^u)\,e^u \\ &= \frac{1}{A(e^{\ln\omega})}A'(e^{\ln\omega})\,e^{\ln\omega} \\ &= \frac{1}{A(\omega)}A'(\omega)\,\omega \\ &= \frac{\omega}{A(\omega)}\frac{dA}{d\omega} \end{aligned}$$

Not so easy to remember!

(b) We consider a linear amplitude spectrum

$$\ln A = m\ln\omega + b \tag{S12}$$

$$g_0(u) = mu + b \tag{S13}$$

$$g_0'(u) = m \tag{S14}$$

$$g_n'(u) = n + m \tag{S15}$$

If $A(\omega)$ is flat, then $m = 0$. Since we are asking for the difference between displacement and velocity, we have $n = 1$. The resulting slope of $A_1(\omega)$ in log space is

$$n + m = 1 + 0 = 1 \tag{S16}$$

(c) In this case, we have $m = -2$ and $n = 2$ (displacement to acceleration), so

$$n + m = 2 + -2 = 0 \tag{S17}$$

So the spectrum of $A_2(\omega)$ is flat in log space.

[2] We will need the chain rule: $h(x) = g(f(x))$, then $h'(x) = g'(f(x))\,f'(x)$. In our case, $h(x) = A(e^x)$, so $g = A$ and $f(x) = e^x$.

Problem 2. Deconvolving the instrument response

1. (See output figures from code.)

2. (a) As shown in the output of the code, the duration of the seismogram is 10.029 days (or 8.665×10^5 s).

   (b) As shown in the output of the code, the time step is $\Delta t = 1$ s.

   (c) The Nyquist frequency is $f_{\text{Nyq}} = 1/(2\Delta t) = 0.5$ Hz.

   (d) Zooming in (Figure S1b), we see that the most conspicuous oscillation is the 12-hour tidal signature.

   (Very roughly, the peak-to-peak period is 0.5×10^5 s, which is 13.9 hours.)

   (e) The largest aftershock occurs around `2005-01-01 06:49:32`. Searching the GCMT catalog reveals that this is a M_{w} 6.7 aftershock:

```
200501010625A OFF W COAST OF NORTHERN
  Date: 2005/ 1/ 1   Centroid Time:  6:25:48.3 GMT
  Lat=   4.97  Lon=  92.22
  Depth= 12.0   Half duration= 5.2
  Centroid time minus hypocenter time:  3.5
  Moment Tensor: Expo=26  -0.052 -0.669 0.721 -0.287 -0.378 -0.854
  Mw = 6.7    mb = 6.0    Ms = 6.7   Scalar Moment = 1.2e+26
  Fault plane:  strike=111    dip=68   slip=-173
  Fault plane:  strike=18    dip=84   slip=-22
```

   (f) This aftershock is a strike slip fault, which is very different from the thrust mechanism of the mainshock. Therefore it is clear that the mainshock triggered earthquakes on other faults. (Alternatively, the mainshock rupture could have included rupture on "minor" strike-slip faults as well.)

   (g) The main features in the 10-day seismogram at Canberra (Figure S1) are:

      i. pre-Sumatra noise
      ii. the Sumatra earthquake
      iii. aftershocks
      iv. a 12-hour (tidal) oscillation (only seen after zooming in; Figure S1b)

3. (a) Figure S2a shows the amplitude spectrum without any log-scaling of either axis. The large peak(s) near $f = 0$ is shown in Figure S2b. These peaks are the tides, with periods of approximately 12 hours and 24 hours.

   (b) The amplitude spectrum of the Canberra time series is shown in Figure S3.

   Note that when we log-scale the frequency values, we will not plot the first entry, which is $f = 0$ Hz. The first nonzero frequency will be $f_2 = \Delta f = 8.53 \times 10^{-7}$, with $\log_{10}(f_2) = -6.02$. So the plotting limits range from about 10^{-6} Hz to 0.5 Hz.

   (c) See Figure S3 for details. The maximum peaks are associated with tides (24-hour and 12-hour periods). See Appendix A for more on tides.

(d) The maximum frequency is the Nyqust frequency, $f_{\rm Nyq} = 1/(2\Delta t) = 0.5$ Hz, where $\Delta t = 1$ s is the sample rate.

(e) The minimum non-zero frequency is determined from the length of the time series and also the sample rate.

If there was no padding of zeros in computing the Fourier transform, then we would have

$$\Delta f = 1/(n\Delta t) = 1/(866508 \times 1) \approx 1.9 \times 10^{-6} \text{ Hz}. \tag{S18}$$

This corresponds to a period of 6.1 days, which is less than the 10-day length of the time series.

In our case, there is some padding of zeros in computing the Fourier transform, which has the effect of creating finer sampling in the frequency domain (since n increases). From `df = f(2) - f(1)` we see that

$$\Delta f = 1/2^{20} \approx 9.5 \times 10^{-7} \text{ Hz}. \tag{S19}$$

This corresponds to a period of 12.1 days, which is slightly more than the 10-day length of the time series.

You can see in `wf_fft.compute` that the key command is `fft(x,NFFT)`, where `NFFT` is set to 2^k, such that $2^{k-1} < n < 2^k$.

4. (a) The top figure in Figure S5 shows a zoom in on Figure S3 but without loglog scaling.

(b) The peaks can be identified in Figure 1 of *Park et al.* (2005). The similarity of the y-axis values suggests that Park is also plotting the amplitude spectrum of the raw time series (in counts). However, they do not list any units or label associated with the y axis.

(c) From *Park et al.* (2005): "For a spherical reference model, all $2l+1$ vibrations of ${}_nS_{lm}$ or ${}_nT_{lm}$ have identical frequency. On the real Earth, departures from the symmetries of a spherical reference model cause its free oscillations to couple, hybridize, and suffer fine-scale splitting of their vibrational frequencies. Frequency splitting of free oscillations with periods $T > 1000$ s is caused mainly by Earth's rotation, similar to Zeeman splitting of electron energies in an external magnetic field."

The ${}_0S_0$ peak at 0.815 mHz (period 20.5 minutes) is the "breathing mode" and is not subject to splitting, since $l = 0$: since $-l \le m \le l$, we must have $m = 0$ only. Other peaks are split due to deviations of from the Spherical Non-Rotating Elastic Isotropic (SNREI) model. For the gravest modes, the frequency deviation of the mth singlet from the $m = 0$ degenerate frequency can be computed as (*Dahlen and Tromp*, 1998, Eq. 14.54)

$$\delta\omega_m = \omega_0(a + bm + cm^2) \qquad -l \le m \le l, \tag{S20}$$

where expressions for a and c are primarily associated with ellipticity (but also large-

scale structure), and b is associated with rotation.

(d) Regarding some of the smallest peaks visible, some of these are toroidal oscillations but observed on this vertical component! From *Park et al.* (2005): "The coupling between spheroidal and toroidal modes associated with Earth's Coriolis force causes them to form hybrid vibrational patterns. The hybridized toroidal modes are predicted to acquire a vertical vibrational component, a feature nominally restricted to spheroidal modes."

5. The top row of Figure S4 shows the instrument response to acceleration over the full range of frequencies that defines the Fourier-transformed seismogram. Note that it is not flat!

   This was addressed in the lab on instrument response (Figure L3).

   The key lines of code are:

```
res = response_get_from_polezero(f,polezero);
Ia = res.values;
figure; loglog(f,abs(Ia)); xlim([min(f) max(f)]);
```

6. Figure S4 shows the amplitude spectrum for the raw time series (like velocity) in comparison with ground acceleration (instrument deconvolved). The effect is to raise the amplitude of the lowest and highest frequencies.

   Figure S5 shows the comparison over the frequency range $[0.2, 1.0]$ mHz. The amplitudes of the lower frequency peaks are higher after deconvolution.

   The key lines of code are:

```
res = response_get_from_polezero(f,polezero);
Ia = res.values;
Xa = C./Ia;
```

   where `C` (which is provided) is $C(\omega) = X_a(\omega)I_a(\omega)$.

7. The caption in Figure 1 in *Park et al.* (2005) states this:

   > Schematic of the motion of free oscillations ${}_0\mathsf{S}_2$, ${}_0\mathsf{T}_2$, ${}_0\mathsf{S}_3$, and ${}_0\mathsf{S}_0$ superimposed on a spectrum computed from 240 hours of vertical seismic motions recorded at the CAN (Canberra, Australia) station of the Geoscope Network. For comparison, fig. S1 plots the acceleration spectrum from the superconducting gravimeter collocated with CAN.

   Our spectrum (Figure S5) does not look exactly like the one in Figure 1 in *Park et al.* (2005). Here are some differences:

   (a) The units on the y axis. There are no units lited in the published figure, so it is hard to say whether the instrument response has been deconvolved. The units are suggestive of counts (Figure S5), though the match is not exact with ours either.

(b) The relative amplitudes of the peaks are different. Our ${}_0\mathsf{S}_0$ peak is by far the largest peak, but this is not the case in the published version.

(c) The smallest peaks, such as ${}_0\mathsf{T}_2$ and ${}_2\mathsf{S}_1$, are more prominent in the published version. If we zoom in on either the amplitude spectrum, or the squared-amplitude spectrum, then we can see that these peaks are indeed present (Figure S6).

Here are some factors that influences the details of a spectrum:

(a) Whether the instrument response was removed. As we saw in Figure S5, this can change the relative (and absolute) amplitudes of the peaks.

(b) The duration of the time window. Both are 10 days (240 hours).

(c) The start time of the time window. Ours is from before the event. They do not state when theirs is. For other stations it makes a big difference whether the direct arrival is included. But there is not an obvious difference between Figure S11c and d.

(d) The sampling rate of the time series. Ours is 1 sps; theirs is not stated.

(e) The taper applied. Ours is a Hanning window; theirs is not stated.

(f) The padding of zeros for the fft. Our function will allow for zero-padding such that the length of the time series is a power of 2.

(g) The station location code. For some stations there are multiple location codes, so it's hard to know which seismogram was used. For example, a deep borehole recorded might be different from a surface recording.

(h) Corrections for changes in atmospheric pressure (*Zürn and Widmer*, 1995). In Note 47, *Park et al.* (2005) states that they do not need to perform an atmospheric correction because the signal-to-noise is high enough.

Problem 3. Spectral analysis of noise

1. It turns out that three days before the Sumatra earthquake there was a M_{w} 8.1 earthquake south of New Zealand on the boundary between the Australia and Pacific plates. As far as I know, no one has published any scientific finding about the connection. See the response from USGS:

   `http://earthquake.usgs.gov/earthquakes/eqinthenews/2004/us2004slav/faq.php`

   The listing from the GCMT catalog is:

```
  122304A NORTH OF MACQUARIE ISLAN
Date: 2004/12/23   Centroid Time: 14:59:30.9 GMT
Lat= -49.91  Lon= 161.25
Depth= 27.5   Half duration=26.7
Centroid time minus hypocenter time: 26.5
Moment Tensor: Expo=28  0.108 0.874 -0.982 0.488 -0.317 -1.210
```

```
Mw = 8.1    mb = 6.5    Ms = 7.7   Scalar Moment = 1.63e+28
Fault plane:  strike=69    dip=74   slip=167
Fault plane:  strike=163    dip=78   slip=16
```

2. Figure S7 shows a 90-hour time series of noise that does not contain any obvious earthquakes. The 12-hour tidal period is the dominant period.

3. (a) Figure S8 compares the amplitude spectrum of noise for the raw time series and for the instrument-deconvolved acceleration.

   (b) The period ranges 5–8 s and 10–16 s mentioned in *Shearer* (2009, Section 11.2) are not exactly aligned with noise spectrum at Canberra. This is not surprising since this is one station at one particular time, whereas the Shearer figure is a global average, presumably over yearly time intervals. The spectral peaks associated with ocean microseisms will depend on the location of the storm that is generating the waves with periods 10–16 s.

   (c) Based on the CAN noise spectrum, we expect the best signal-to-noise ratio at frequencies near the Nyquist and also over the period range 50–500 s

Problem 4. Spectral analysis of the Sumatra earthquake recorded at Canberra

1. Figure S10 shows amplitude spectra for five different time series:

   - (a) P wave, 600 seconds.
   - (b) Direct arrival (P wave to R1 Rayleigh), 4 hours.
   - (c) Modes, from 1 day after the event to 10 days after the event.
   - (d) Full 10-day seismogram, including direct arrival.
   - (e) Noise spectrum for a 4-day time window before the event.

   In Figure S11 we zoom in on the frequency range $[0.2, 1.0]$ mHz. As expected, the lowest mode peaks are only resolved with the multi-day time series. Including the direct arrival does not have a significant effect on the modes spectra (c vs d).

   (a) Figure S10.

   (b) The frequencies associated with the maximal amplitudes correspond to periods between 15 and 25 s. These are surface waves (Rayleigh waves, since this is the vertical component).

   (c) Comparing Figure S10b vs Figure S10e, we see that both the direct arrival and the noise spectra decay toward the Nyquist frequency of 0.5 Hz. The direct spectrum has the highest amplitudes in a region where the noise spectrum is relatively low, that is, below the frequencies of the ocean microseism bands. The direct spectrum cannot resolve the lowest frequencies (tides and lowest modes) due to the too-short duration (4 hours) of the time series.

(d) Comparing Figure S10b vs Figure S10d, we see that the modes peaks (and tides peaks) are not visible. Also, there is a relatively greater portion of high-frequency content in the 10-day spectrum, but this is probably the signature of background noise.

There is a hint of three modes peaks from the direct arrival spectrum in Figure S11b. You can imagine the transition from Figure S10b to Figure S10d as the time series is extended from 3 hours after the origin time to 10 days after the origin time. The peaks will sharpen up!

2. (a) Supplemental Figure S11 of *Ammon et al.* (2005) shows that the P wavetrains are approximately 500 s long. This is easier to see when looking at all three components, since the horizontal components reveal the dominant S arrival (Figure S12). Figure S13a shows the P wave at CAN.

   (b) Figure S13b shows the amplitude spectrum of the P wave at CAN.

   (c) *Stein and Wysession* (2003, p. 267) show a couple different ways to estimate the corner frequency. Figure S13 shows their model applied to the Canberra P spectrum. This suggests a rupture time of 6.0 s, a rise time of 0.80 s, and a corner frequency of 0.145 Hz (6.9 s). It is quite possible that this simple model does not apply for such long ruptures.

3. (a) Figure S14b shows the 2–4 Hz band-passed seismogram. Figure S15 shows a zoomed-in version, which we use to estimate a rupture duration of 650 s.

   Figure S16 shows the processing steps of *Ni et al.* (2005) to get the envelope of the high-frequency signal.

   (b) Following the main pulse (Figure S14b) there are some odd signals that all have the same amplitude but which occur during the main arrival of the earthquake waves.

   Figure S17, filtered at 4–8 Hz, shows that the bursts coincide with the phase of the dominent-period (10–30 s) surface waves.

References

Ammon, C. J., et al. (2005), Rupture process of the 2004 Sumatra-Andaman earthquake, *Science*, *308*, 1133–1139.

Dahlen, F. A., and J. Tromp (1998), *Theoretical Global Seismology*, Princeton U. Press, Princeton, New Jersey, USA.

Kvale, E. P., H. R. Johnson, C. P. Sonett, A. Archer, and A. Zawistoski (1999), Calculating lunar retreat rates using tidal rhythmites, *J. Sed. Res.*, *69*, 1154–1168.

Ni, S., D. Helmberger, and H. Kanamori (2005), Energy radiation from the Sumatra earthquake, *Nature*, *434*, 582.

Park, J., et al. (2005), Earth's free oscillations excited by the 26 December 2004 Sumatra Andaman earthquake, *Science*, *308*, 1139–1144.

Shearer, P. M. (2009), *Introduction to Seismology*, 2 ed., Cambridge U. Press, Cambridge, UK.

Stein, S., and M. Wysession (2003), *An Introduction to Seismology, Earthquakes, and Earth Structure*, Blackwell, Malden, Mass., USA.

Zürn, W., and R. Widmer (1995), On noise reduction in vertical seismic records below 2 mHz using local barometric pressure, *Geophys. Res. Letters*, *22*(24), 3537–3540.

A Tides tables

Table S1: Fundamental periods of the earth's and the moon's *orbital* motion. The five angular frequencies, ω_i, are used in defining the tidal cycles in Tables S3 and S4. The perihelion is the solar perigee.

Period, T	Angular frequency, ω $360°/T$ (deg/day)	(rad/s)	Nomenclature
27.321 582 days	13.176 397	$\omega_1 = 2.6617 \times 10^{-6}$	Period of lunar declination
365.242 199 days	0.985 647	$\omega_2 = 1.9911 \times 10^{-7}$	Period of solar declination
8.847 years	0.111 410	$\omega_3 = 2.2505 \times 10^{-8}$	Period of lunar perigee rotation
18.613 years	0.052 954	$\omega_4 = 1.0697 \times 10^{-8}$	Period of lunar node rotation
20 940 years	0.000 047 070	$\omega_5 = 9.5084 \times 10^{-12}$	Period of perihelion rotation

Table S2: Fundamental periods of the earth's *rotational* motion.

Period, T (hours)	Angular frequency, ω $360°/T$ (deg/hour)	(rad/s)	Expression	Nomenclature
23.934	15.041 07	7.2921×10^{-5}	ω_0	lunar-solar declinational
24	15	7.2722×10^{-5}	$\omega_S = \omega_0 - \omega_2$	basic solar
24.841	14.492 05	7.0259×10^{-5}	$\omega_M = \omega_0 - \omega_1$	basic lunar

Table S3: Tidal cycles, measured from the tidal spectrum of the earth's oceans. The table is divided into semidiurnal cycles (1–4), diurnal cycles (5–8), and long-period cycles (9–15). Periods are calculated from the expressions listed in Table S4. Names reflect the preferred usage of tidal sedimentation studies (e.g., *Kvale et al.*, 1999).

Name	Label	Period, $T = 2\pi/\omega$	
		days	hours
declinational	K_2	0.4986	11.967
basic solar	S_2	0.5000	12.000
basic lunar	M_2	0.5175	12.421
elliptical (to M_2)	N_2	0.5274	12.658
declinational	K_1	0.9973	23.934
basic solar	P_1	1.0028	24.066
basic lunar	O_1	1.0758	25.819
elliptical (to O_1)	Q_1	1.1195	26.869
tropical (declinational to M_0)	$T\ (Mf)$	13.661	163.932
synodic (variational, lunar)	S	14.765	177.180
anomalistic (elliptical to M_0)	$A\ (Mm)$	27.555	330.660
evectional	E	31.812	381.744
semiyearly (declinational to S_0)	$SY\ (SSa)$	182.621	2191.452
yearly (solar elliptical)	Y	365.260	4383.120
nodal (lunar)	N	18.613 years	

Table S4: Continuation of Table S3. The frequencies ω_i are listed in Tables S1 and S2. Amplitude coefficients are listed for $c > 0.05$.

Label	Angular frequency, ω			Coefficient, c
	Expression	deg/hour	rad/s	
K_2	$2\omega_0$	30.08214	1.458452×10^{-4}	0.1151
S_2	$2\omega_S$	30	1.454441×10^{-4}	0.4229
M_2	$2\omega_M$	28.98410	1.405144×10^{-4}	0.9081
$N_2 = M_2 - A$	$2\omega_M - (\omega_1 - \omega_3)$	28.43973	1.378835×10^{-4}	0.1789
K_1	ω_0	15.04107	7.292259×10^{-5}	0.5305
P_1	$\omega_S - \omega_2$	14.95893	7.252261×10^{-5}	0.1755
O_1	$\omega_M - \omega_1$	13.94304	6.759864×10^{-5}	0.3769
$Q_1 = O_1 - A$	$\omega_M - 2\omega_1 + \omega_3$	13.39866	6.495940×10^{-5}	0.0722
$T\ (Mf)$	$2\omega_1$	1.0980330	5.323333×10^{-6}	0.1564
S	$2(\omega_1 - \omega_2)$	1.0158958	4.925300×10^{-6}	—
$A\ (Mm)$	$\omega_1 - \omega_3$	0.54437	2.639639×10^{-6}	0.0825
$E = S - A$	$\omega_1 - 2\omega_2 + \omega_3$	0.4715211	2.285994×10^{-6}	—
$SY\ (SSa)$	$2\omega_2$	0.08214	3.982130×10^{-7}	0.0729
Y	$\omega_2 - \omega_5$	0.0410667	1.990967×10^{-7}	—
N	ω_4	0.00221	1.069665×10^{-8}	0.0655

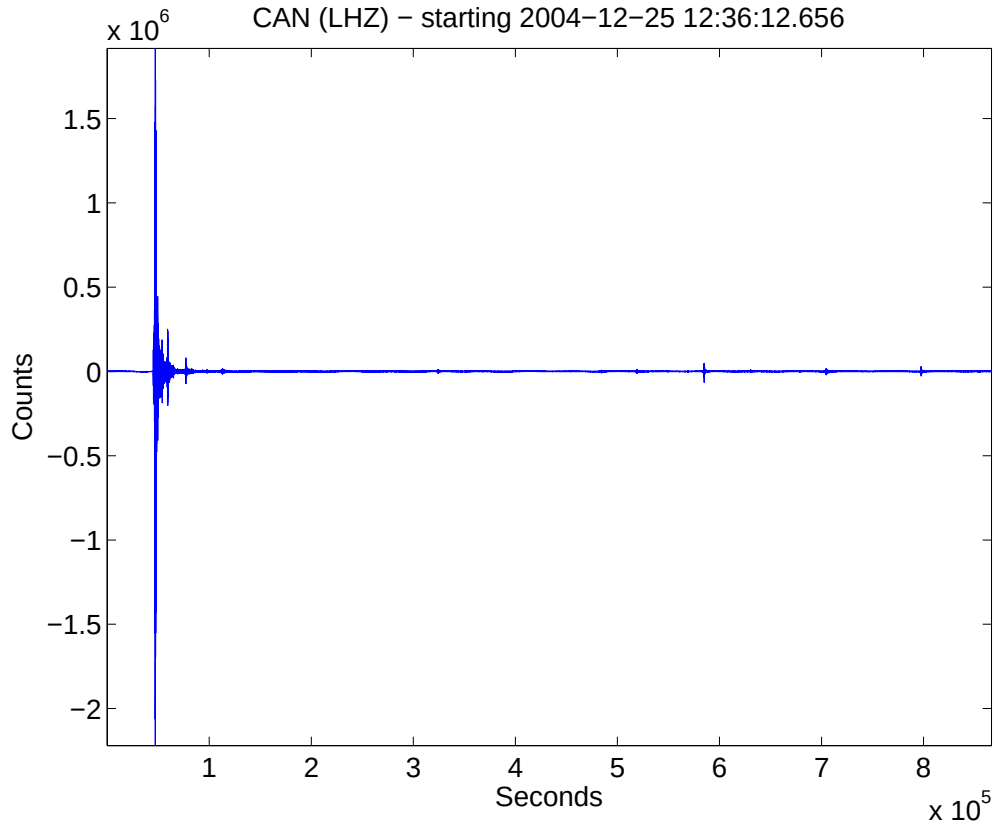

(a)

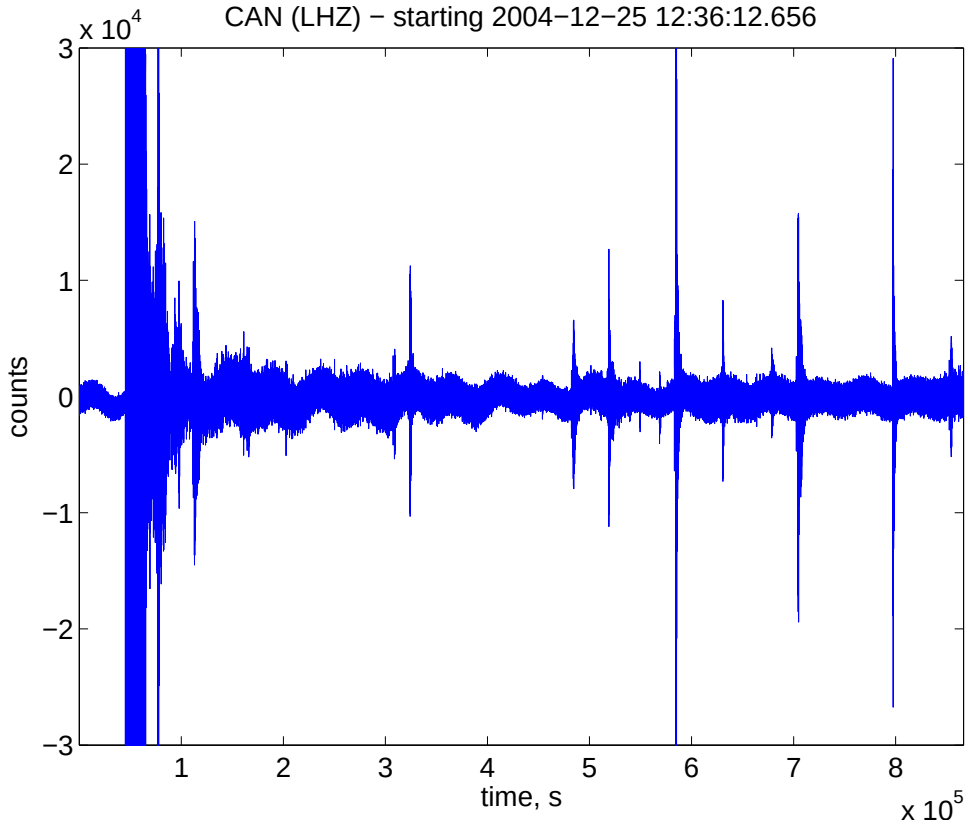

(b)

Figure S1: A 10-day time series including the 2004-12-26 M_{w} 9.2 Sumatra earthquake. (a) Plotted so that Sumatra signal is on scale. (b) Zoom-in on the y-axis, showing that the record is dominated by aftershocks (spikes) and a ∼12-hour period of tides. The largest aftershock is M_{w} 6.7 and occurred on 2005-01-01.

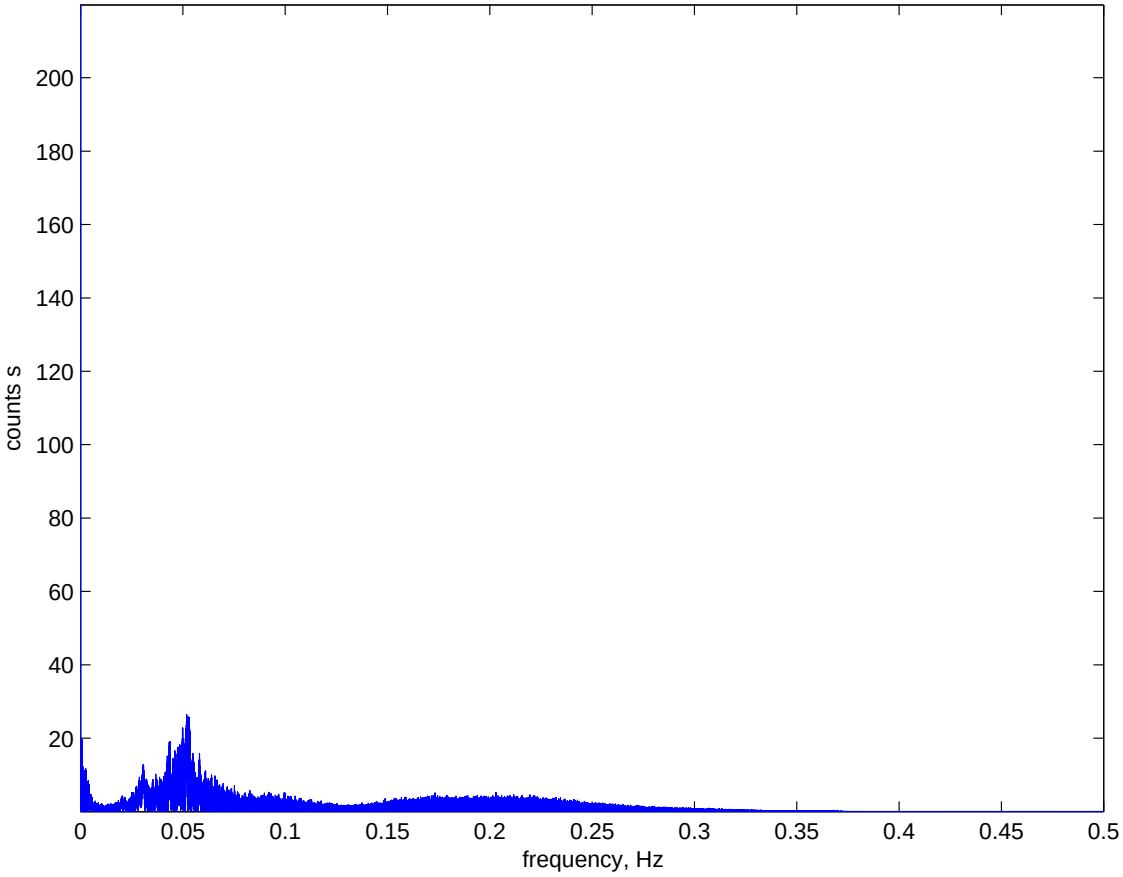

(a)

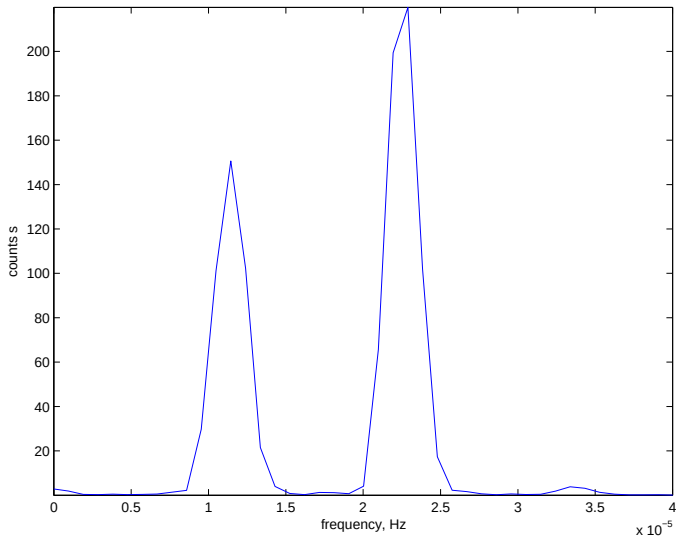

(b)

Figure S2: (a) Amplitude spectrum of the 10-day time series from Canberra, including the main arrival. (b) Zoom-in on the lowest frequencies, which reveal two tidal peaks: the ∼24-hour dirunal tide (left) and the ∼12-hour semidiurnal tide (right).

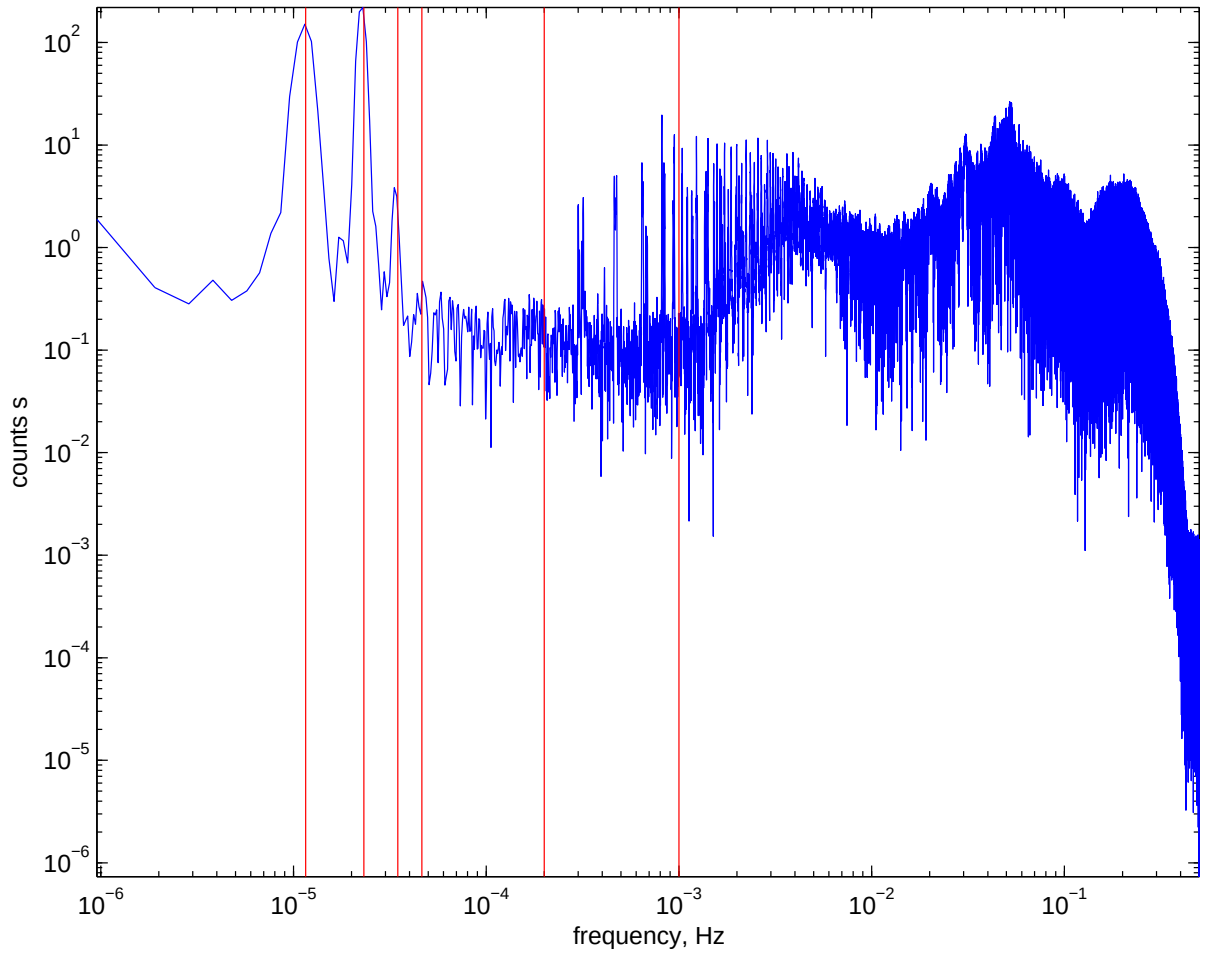

Figure S3: Same as Figure S2, but plotted with log-log scaling. Amplitude spectrum of the 10-day time series from Canberra, including the main arrival. The first four spikes are for kf_0, where $f_0 = 1/(24 * 3600) = 1.1574 \times 10^{-5}$ Hz is the diurnal (24-hour) period and $k = 1, 2, 3, 4$. The first two peaks are the expected tidal periods of 24 and 12 hours. It is unclear (to me) what the third and fourth peaks are (periods 8 and 6 hours), but presumably they are tidal harmonics (e.g., see Appendix A). The frequency range of $[1, 2]$ mHz is also shown (between rightmost vertical lines); the mode peaks are visible in this range.

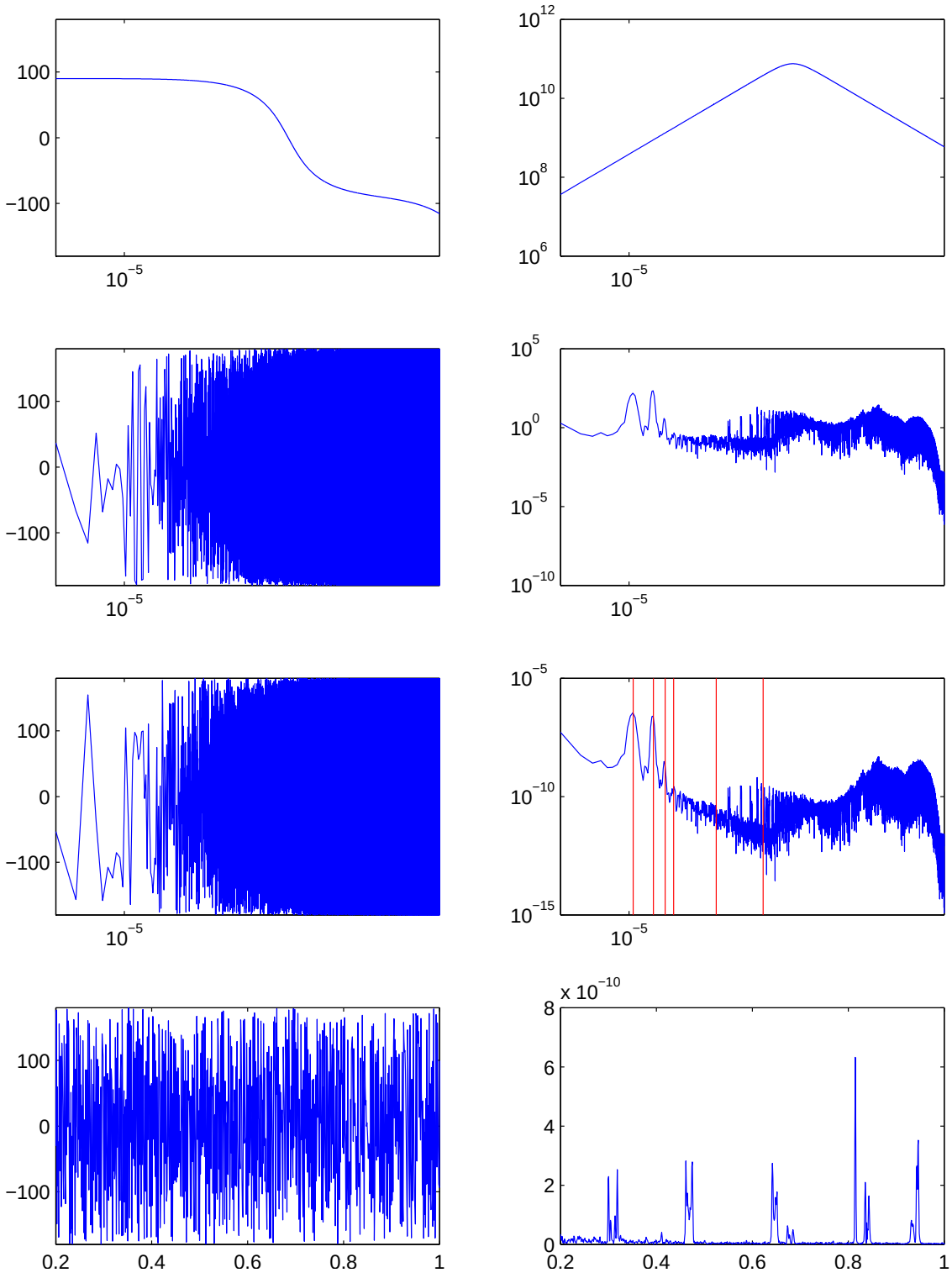

Figure S4: Procedure of deconvolving the instrument response to obtain the spectral ground acceleration. The top row is the instrument response to acceleration. The second row is the phase and amplitude spectrum for the raw time series. The third row shows the spectral acceleration, which is zoomed-in in the bottom row.

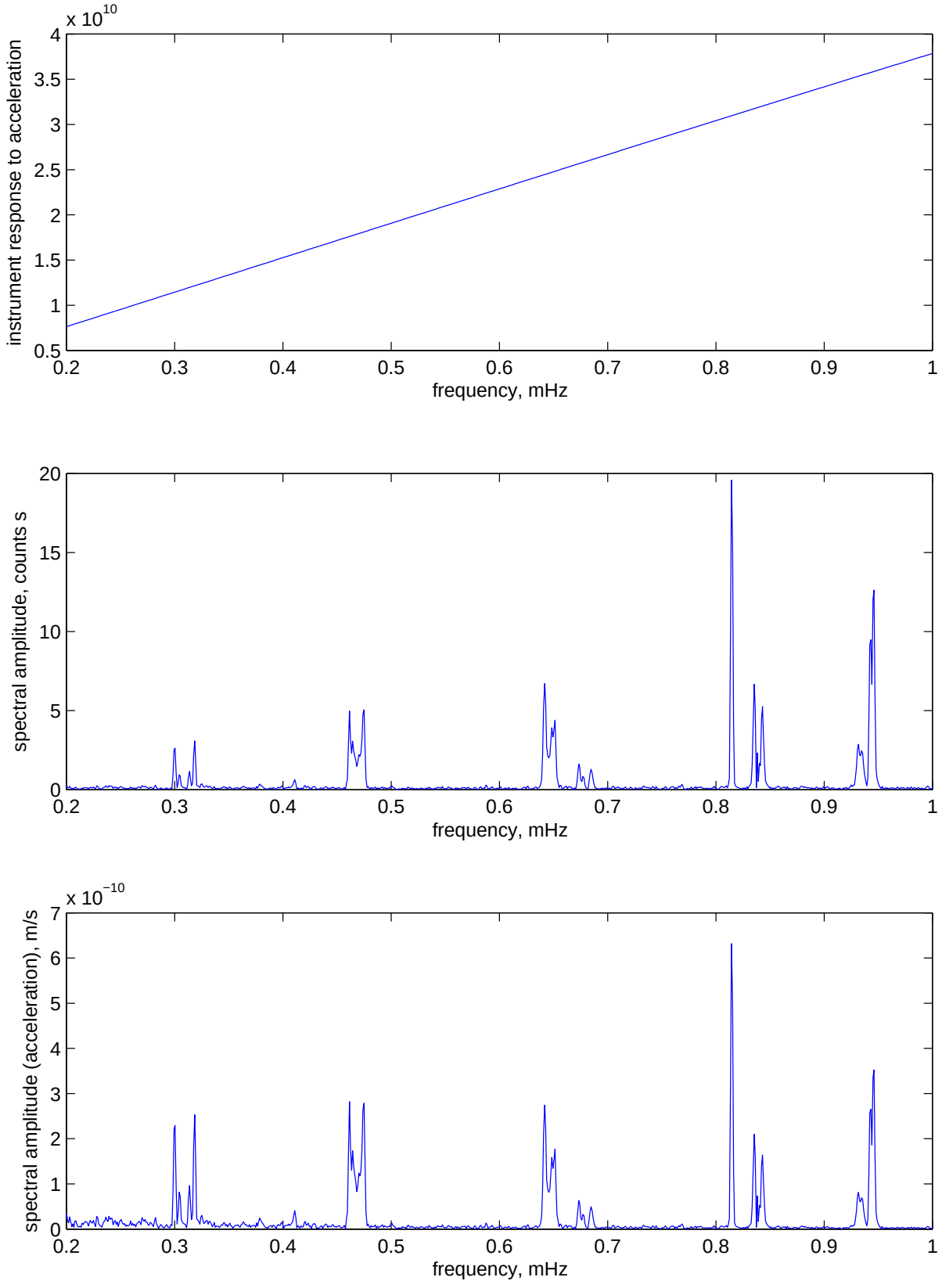

Figure S5: Direct comparison between the amplitude spectrum of the raw time series (middle) and of the ground acceleration (bottom). Notice that the amplitude of the lowest-frequency modes are increased relative to the amplitude of the higher-frequency modes. This is a direct consequence of the linear instrument response over this frequency range (top). This same spectrum is shown in *Park et al.* (2005, Figure 1).

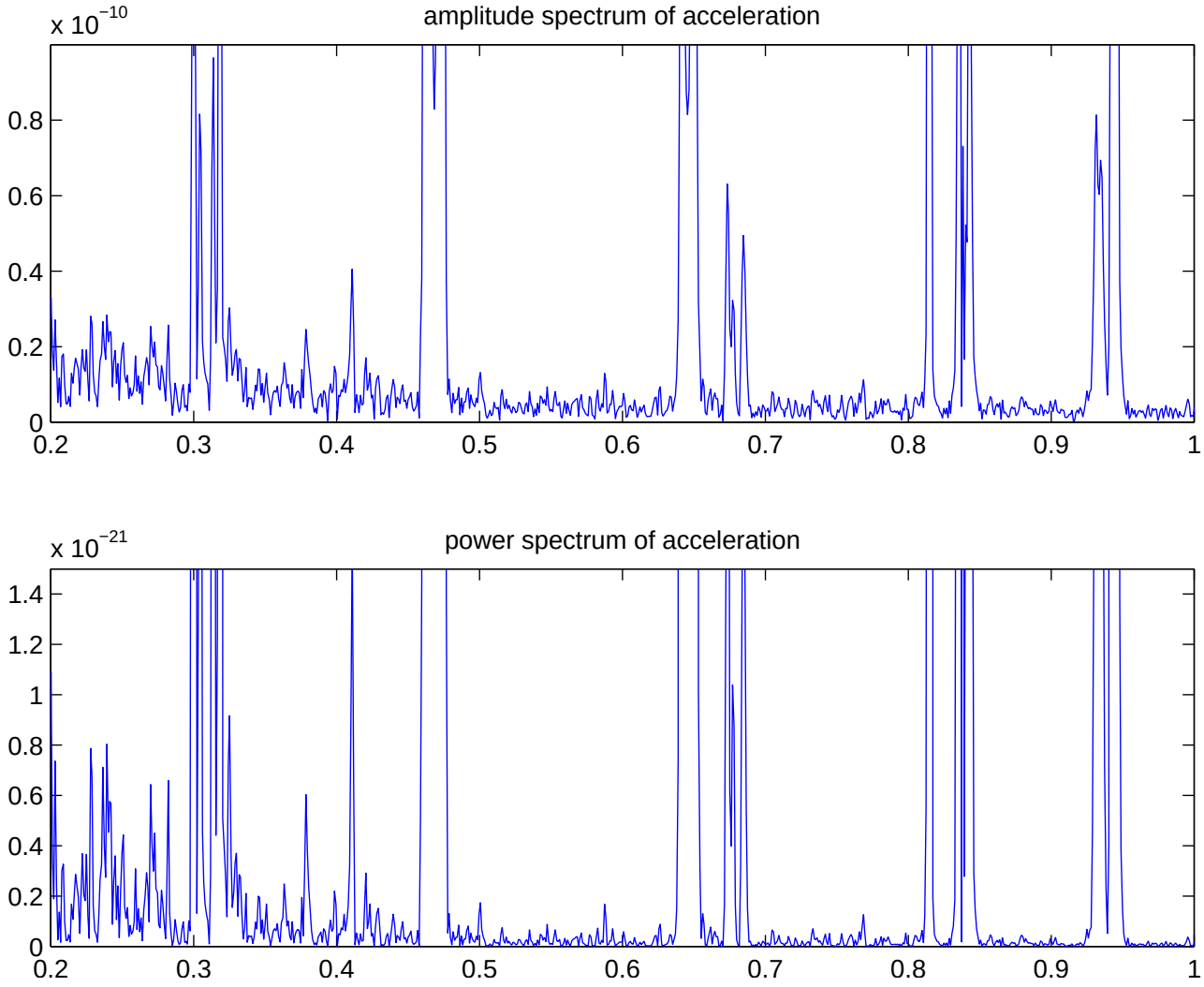

Figure S6: Zoom-in on the amplitude spectrum (Figure S5) to show the smaller peaks. The top shows an amplitude spectrum, and the bottom shows a power spectrum, which is the square of the amplitude spectrum.

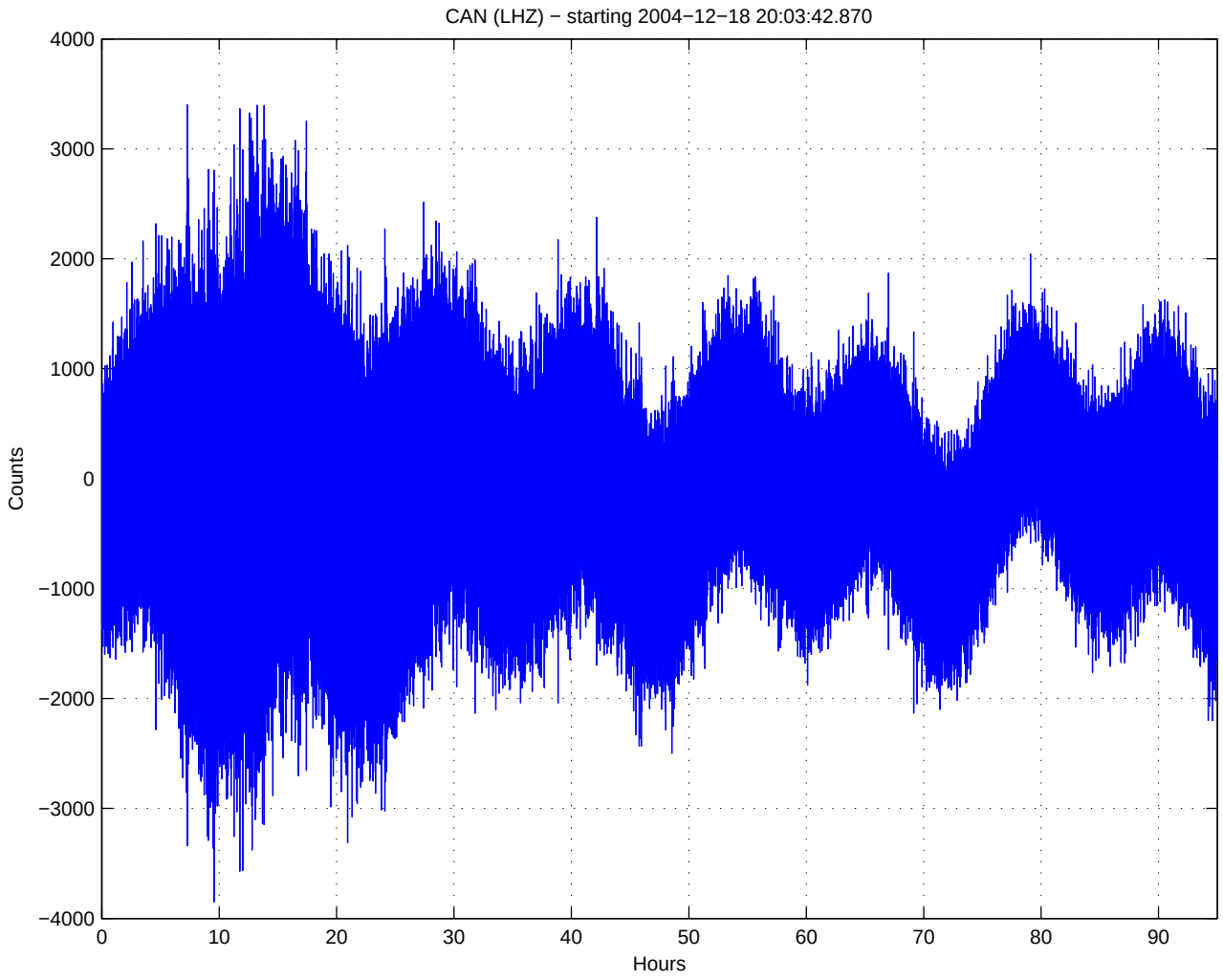

Figure S7: A ∼90-hour time window of "noise" at Canberra in the 10 days before the Sumatra earthquake. The 12-hour tidal period is conspicuous.

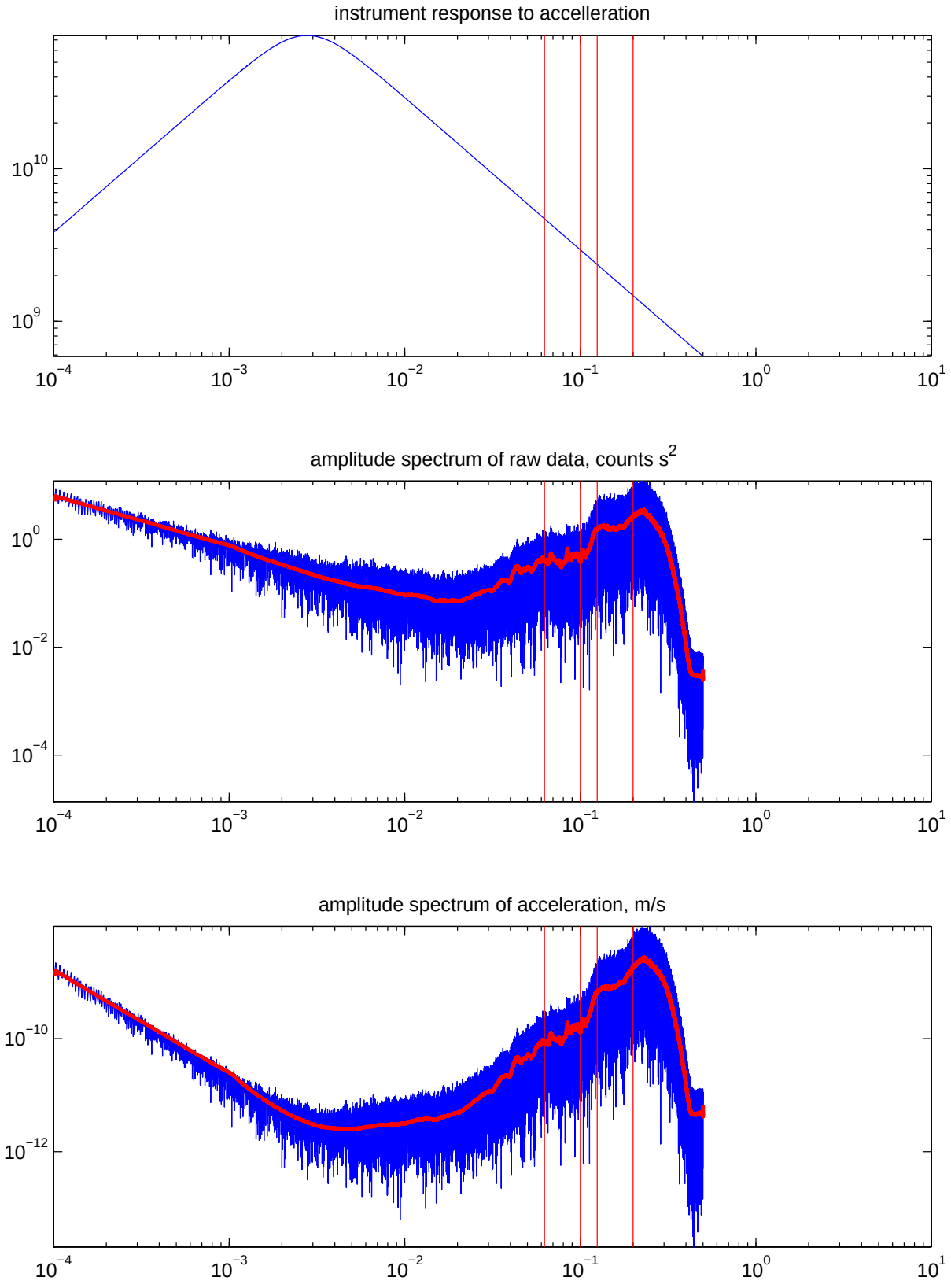

Figure S8: Amplitude spectra of the raw time series in Figure S7. The top shows the instrument response to acceleration, I_a. The middle is the spectrum for the raw time series, C. The bottom is the acceleration spectrum, $X_a = C/I_a$. The vertical bars mark the two ocean microseism period bands of 5–8 s and 10–16 s. The high-frequency limit is determined by the Nyquist frequency of the time series, which is $f_{\mathrm{Nyq}} = 0.5$ Hz for the 1 sample-per-second time series (LHZ).

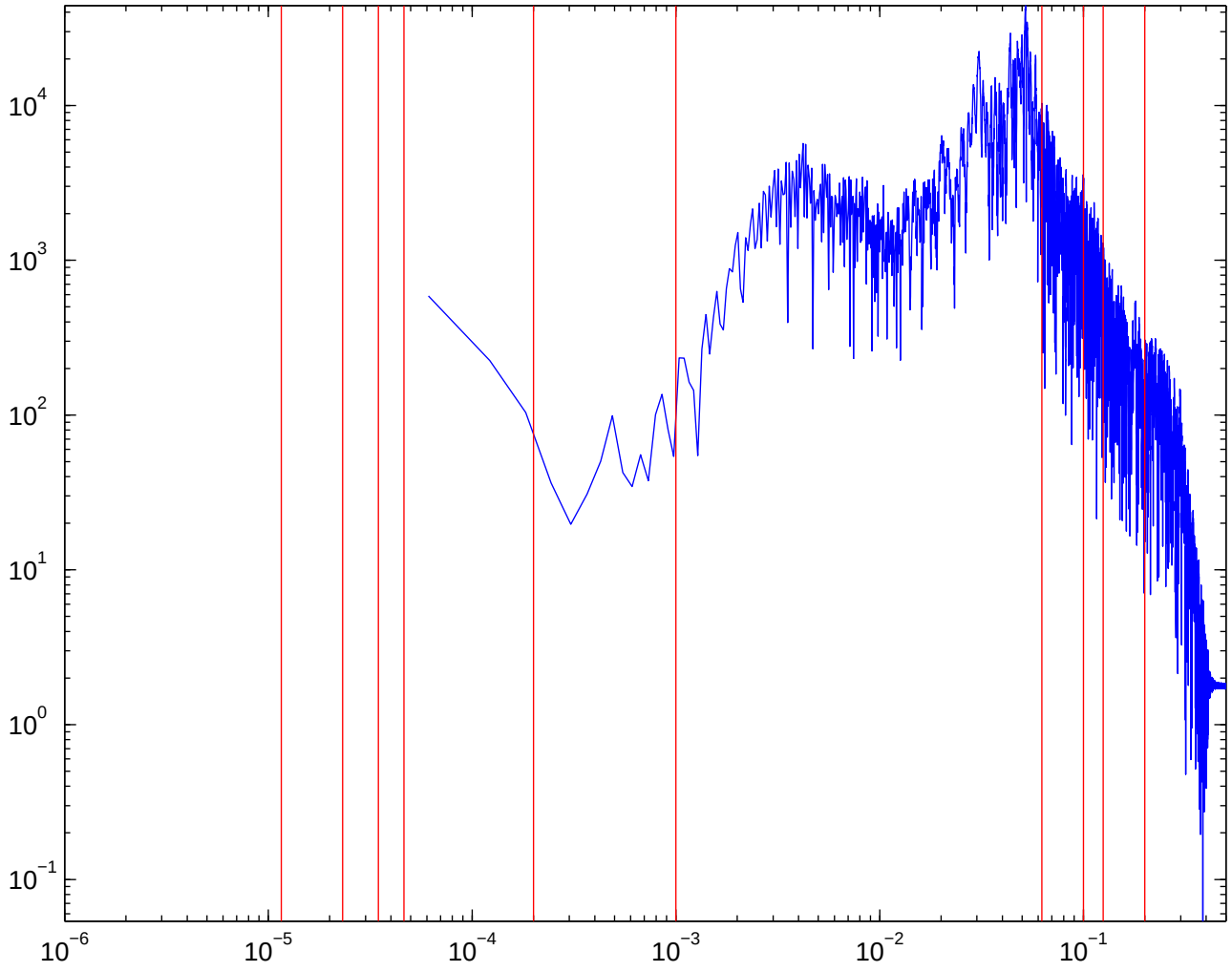

Figure S9: Amplitude spectra for the direct Sumatra wavetrain at CAN (1 hour of noise + 3 hours). The ten vertical lines mark: the tidal frequencies (left four), the modes range $[0.2, 1.0]$ mHz (middle two), and the two ocean microseism bands (right four), 5–8 s and 10–16 s.

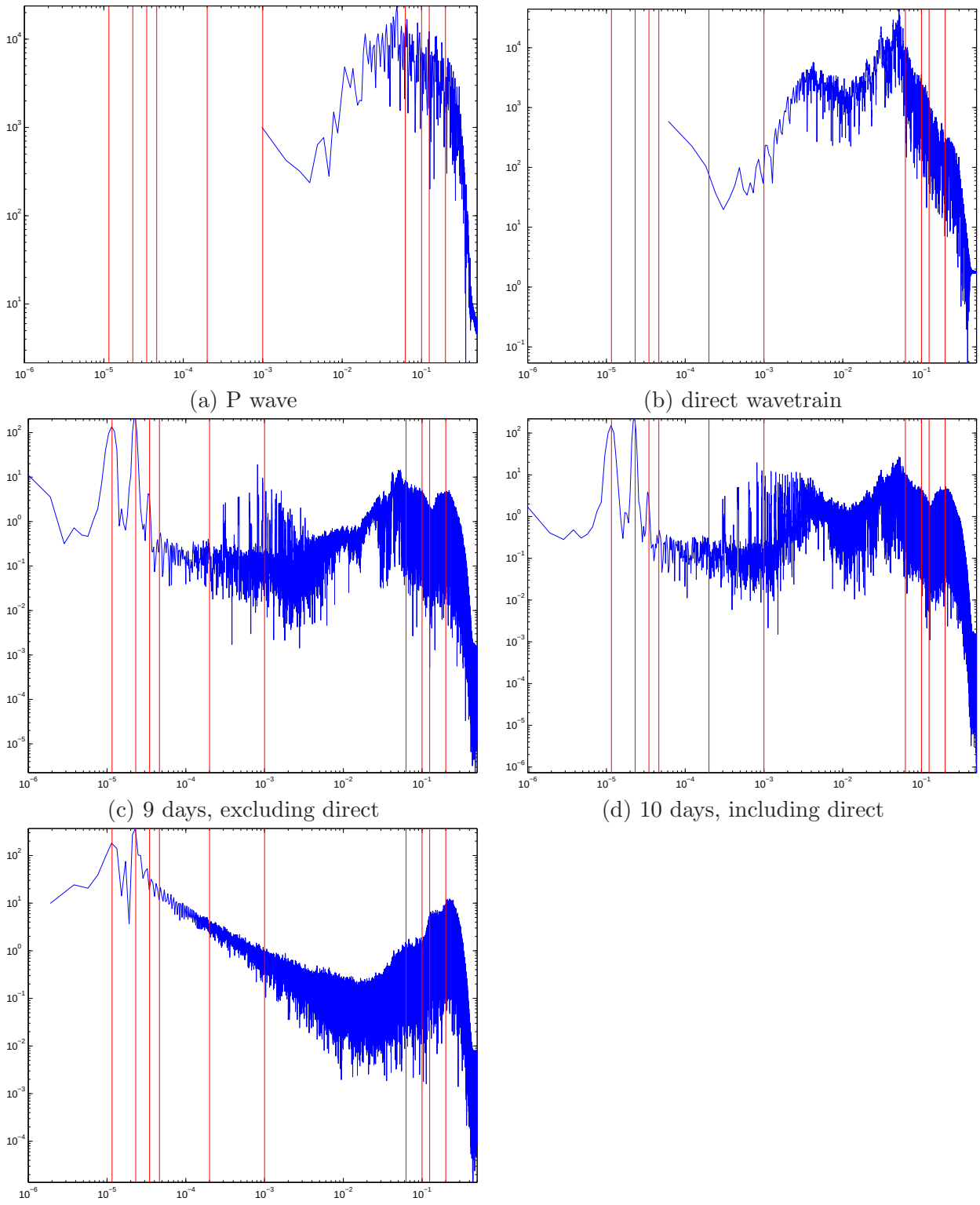

(a) P wave

(b) direct wavetrain

(c) 9 days, excluding direct

(d) 10 days, including direct

(e) noise (4-day time period before Sumatra)

Figure S10: Amplitude spectra for various CAN time series: (a) P wave, (b) direct wavetrain, (c) 9 days, excluding direct, (d) 10 days, including direct. These can be compared with an earthquake-free spectrum, as shown in (e). The ten vertical lines mark: the tidal frequencies (left four), the modes range $[0.2, 1.0]$ mHz (middle two), and the two ocean microseism bands (right four), 5–8 s and 10–16 s.

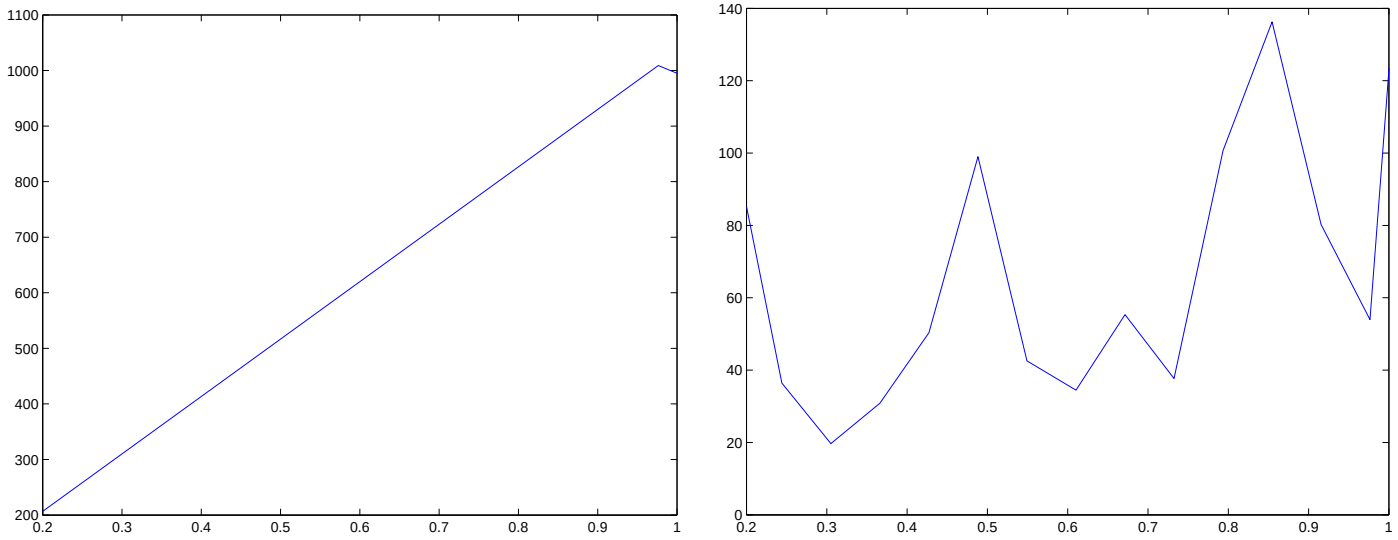

(a) P wave

(b) direct wavetrain

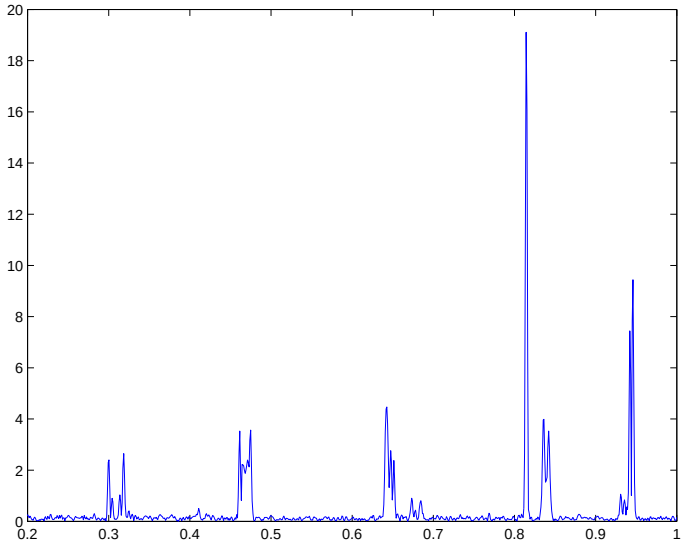

(c) 9 days, excluding direct wavetrain

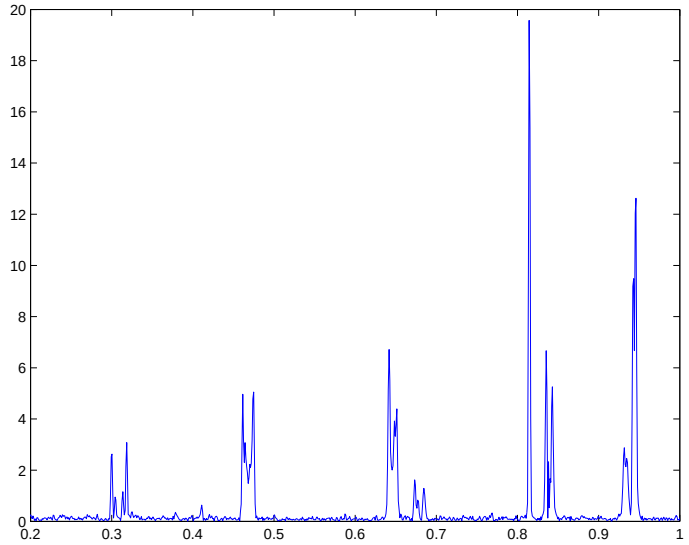

(d) 10 days, including direct wavetrain

Figure S11: Zoom-in on the $[0.2, 1.0]$ mHz region of the spectra in Figure S10.

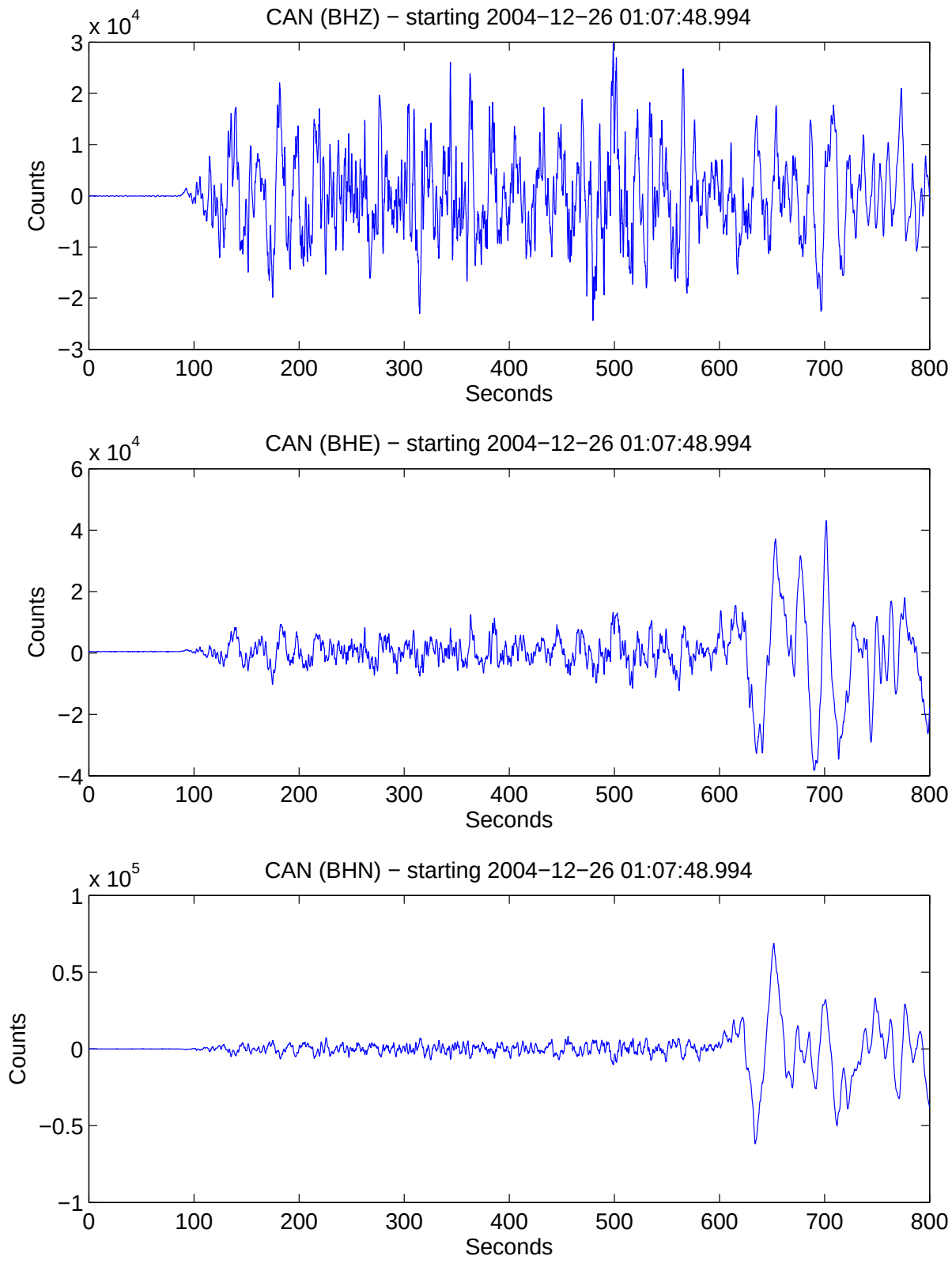

Figure S12: "P wave" recorded at Canberra on the vertical (top), east (middle), and north (bottom) components. The arrival of the (first) S wave is most conspicuous on the horizontal components.

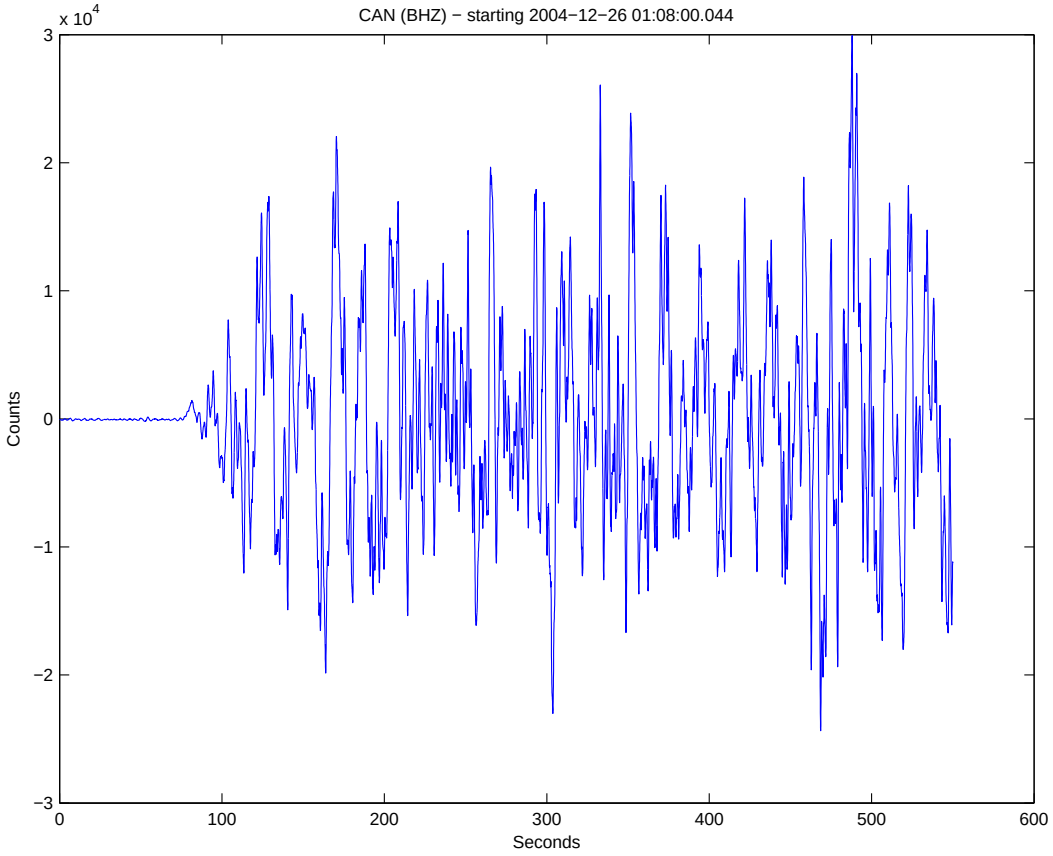

(a)

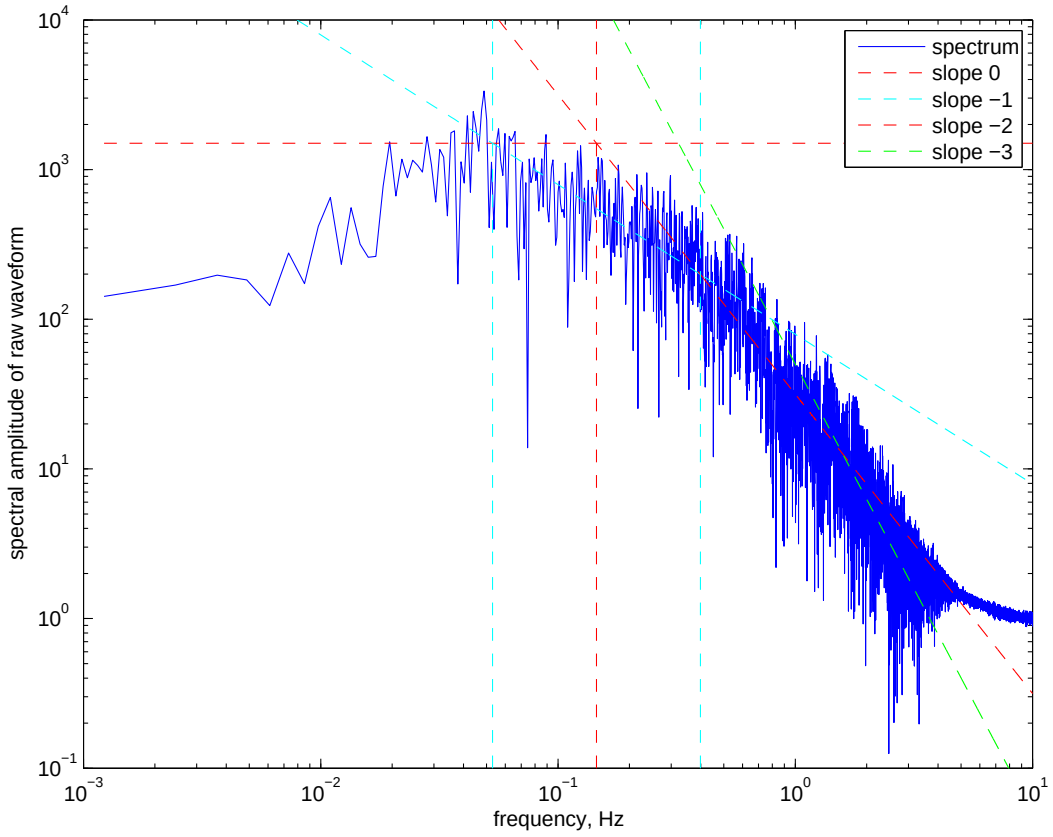

(b)

Figure S13: "P wave" recorded at Canberra in the time domain (a) and the frequency domain (b). The wavetrain is approximately 500 seconds long. The dashed lines on the spectrum show approximate fits for slopes of 0, −1, −2, and −3 in log-log space.

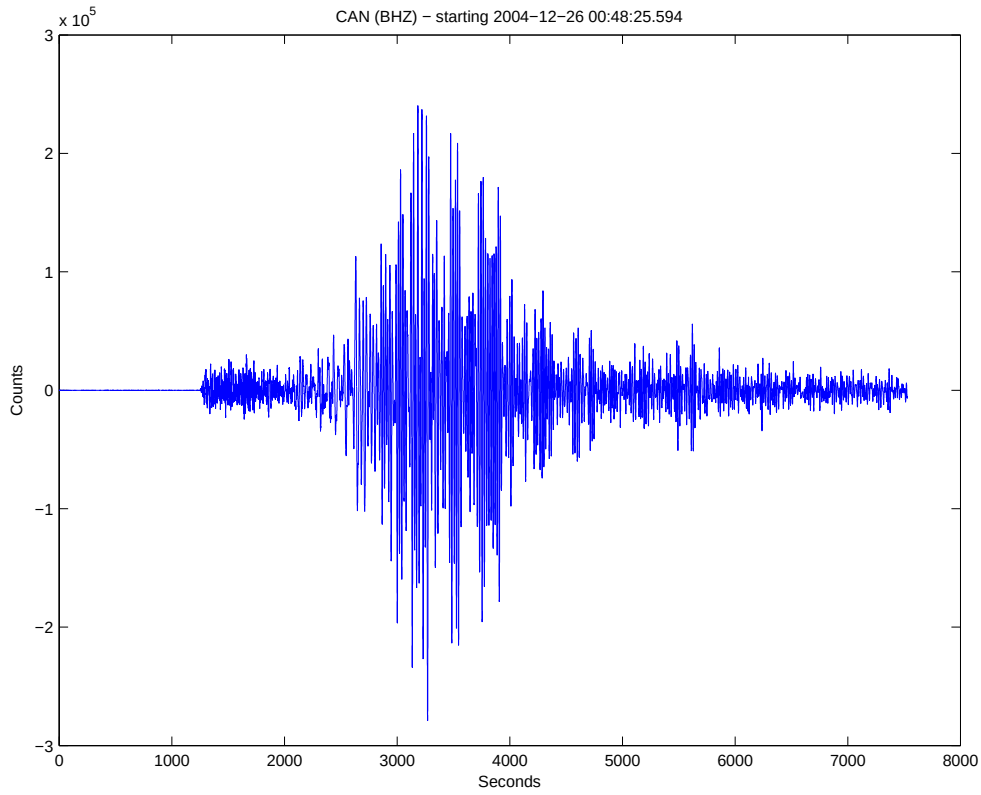

(a)

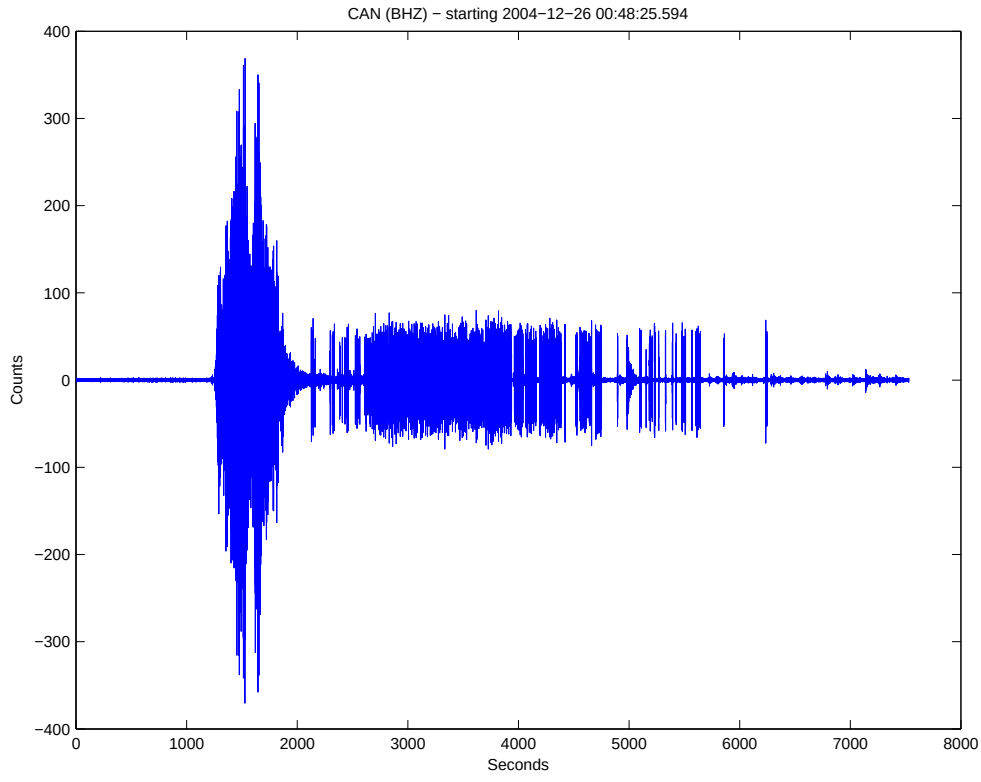

(b)

Figure S14: Full Sumatra arrival at Canberra plotted in raw form (a) and bandpassed over the frequency range 2–4 Hz (b).

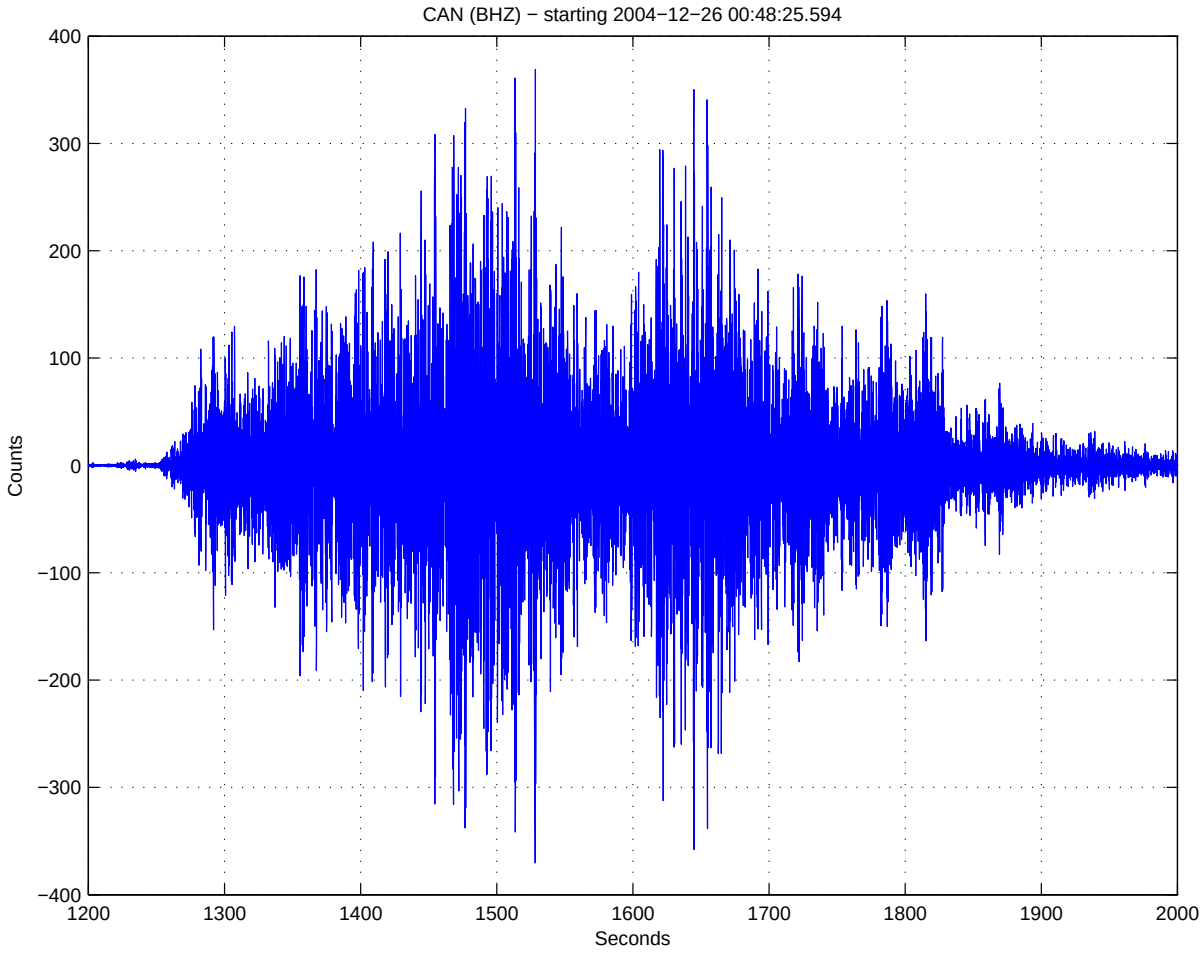

Figure S15: Zoom-in on Figure S14b, which can is used to estimate the rupture duration. If we pick $t_1 = 1250$ s and $t_2 = 1900$ s, then the duration is 650 s.

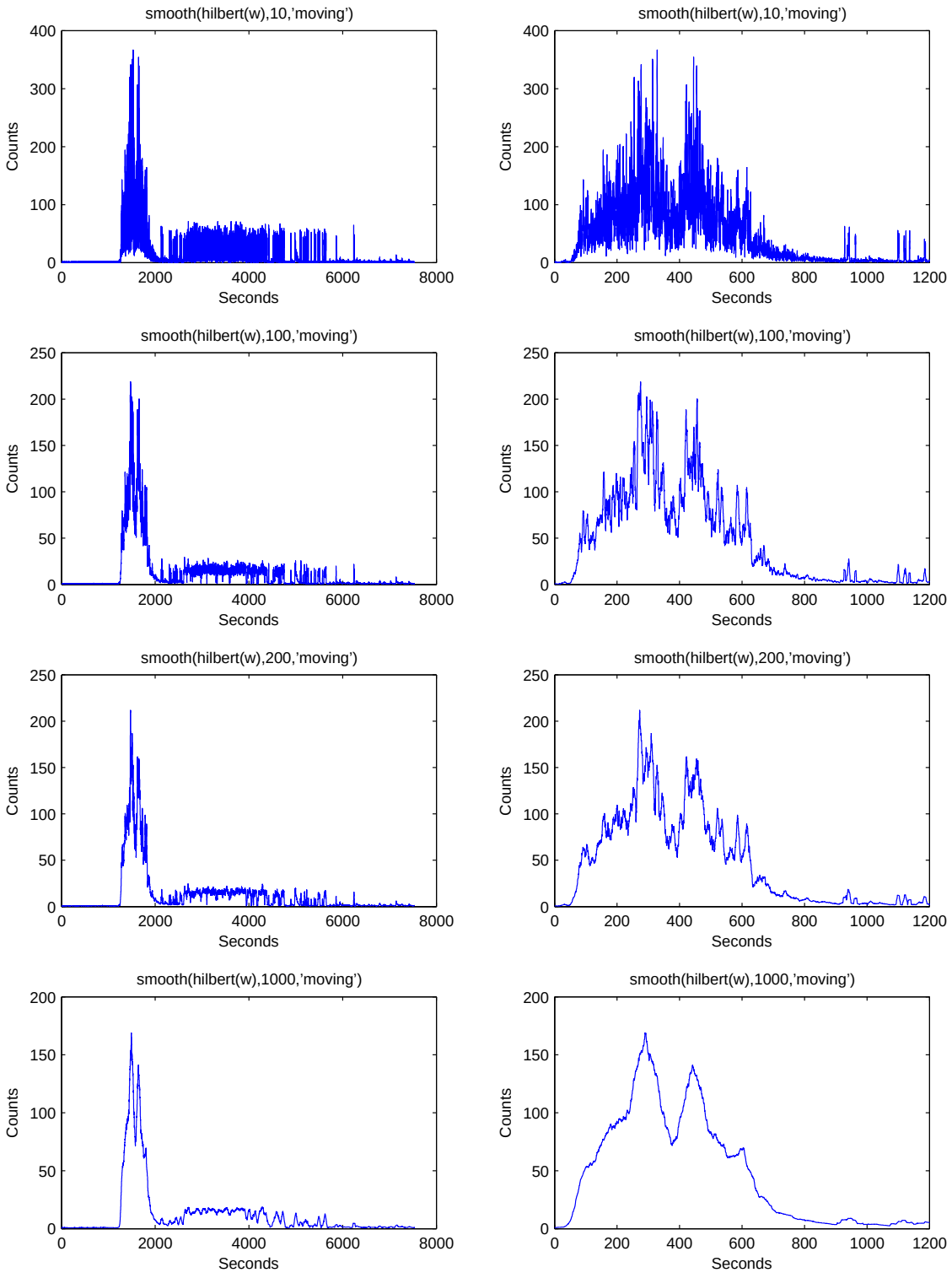

Figure S16: Smoothed Hilbert-transformed time series bandpassed 2–4 Hz. The left column shows the full 8000-second time series; the right column shows the zoom-in on a 1200-second portion, similar to the example in *Ni et al.* (2005). Each row illustrates a different level of smoothing, represented by the number of points in the smoothing filter (10, 100, 200, 1000).

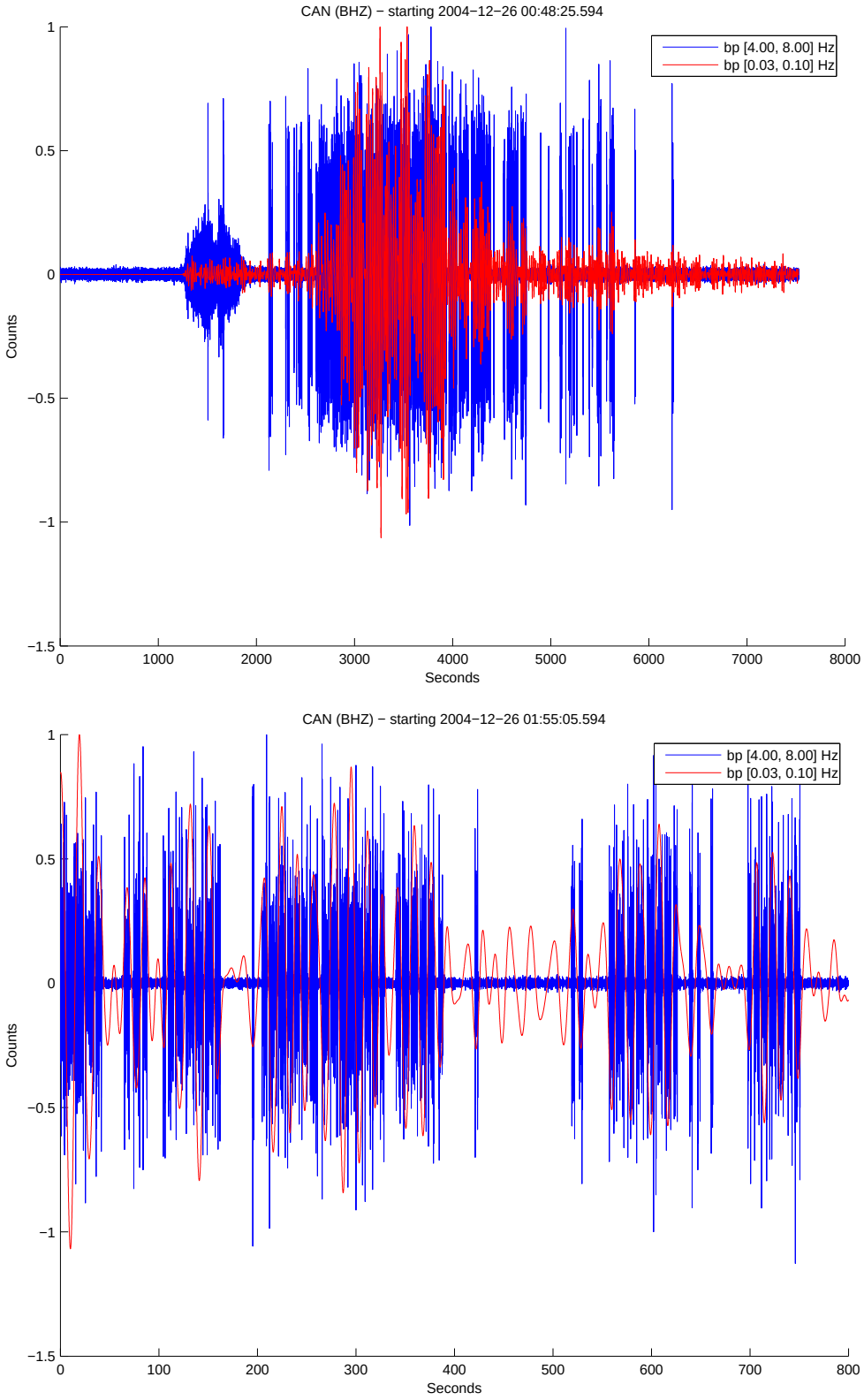

Figure S17: Exploration of the odd-looking high-frequency signals following the main rupture. The blue bandpass is for 4–8 Hz, while the red bandpass is for 0.033–0.1 Hz (10–30 s). Time series have been normalized to the maximum value within each time window. It is apparent that the "bursts" of high-frequency energy occur with the highest amplitudes of the long-period signal. In particular, when the long-period signal is weak, there are fewer high-frequency bursts.